Since January 2020 Elsevier has created a COVID-19 resource centre with free information in English and Mandarin on the novel coronavirus COVID-19. The COVID-19 resource centre is hosted on Elsevier Connect, the company's public news and information website.

Journal of Electroanalytical Chemistry 895 (2021) 115422

Contents lists available at ScienceDirect

Journal of Electroanalytical Chemistry

journal homepage: www.elsevier.com/locate/jelechem

Innovative electrochemical sensor for the precise determination of the new antiviral COVID-19 treatment Favipiravir in the presence of coadministered drugs

Mona A. Mohamed [a,b,1], Ghada M.G. Eldin [a,1], Sani M. Ismail [b], Nadia Zine [b], Abdelhamid Elaissari [b], Nicole Jaffrezic-Renault [b,*], Abdelhamid Errachid [b,*]

[a] Pharmaceutical Chemistry Department, National Organization for Drug Control and Research, Egyptian Drug Authority, Giza, Egypt
[b] Institut de Sciences Analytiques (ISA)-UMR 5280, Université Claude Bernard Lyon 1, 5 rue de la doua, 69100 Lyon, France

ARTICLE INFO

Keywords:
COVID 19
Favipiravir
Graphene derivatives
Real sample analysis

ABSTRACT

Due the current pandemic of COVID-19, an urgent need is required for serious medical treatments of a huge number of patients. The world health organization (WHO) approved Favipiravir (FAV) as a medication for patients infected with corona virus. In the current study, we report the first simple electrochemical, greatly sensitive sensor using MnO_2-rGO nanocomposite for the accurate determination of Favipiravir (FAV). The developed sensor showed a high improvement in the electrochemical oxidation of FAV comparing to the unmodified screen-printed electrode (SPE). The suggested platform constituents and the electrochemical measurements parameters were studied. Under optimal experimental parameters, a current response to the concentration change of FAV was found to be in the linear range of 1.0×10^{-8}–5.5×10^{-5} M at pH 7.0 with a limit of detection 0.11 μM and a quantification limit of 0.33 μM. The developed platform was confirmed by the precise analysis of FAV in real samples including dosage form and plasma. The developed platform can be applied in different fields of industry quality control and clinical analysis laboratories for the FAV determination.

1. Introduction

During the year 2020, the world faced the worst public-health crisis in past hundred years, COVID-19 pandemic. Coronaviruses are large genome viruses of the *Nidovirales* order, with a positive-strand RNA [1]. European and almost all countries have applied non-pharmaceutical involvements, like school closure and national lockdown that lead to huge economic crises [2]. Regardless of the major efforts to stop its spread, COVID-19 has affected considerable health and financial burden, stressing the urgent need for antiviral treatments [1]. Great efforts have been devoted to the development of an antiviral agent for the halt of the progression of this ailment. During the pandemic influenza in Japan 2014, Favipiravir (FAV) was approved for the treatment of that ailment which showed high potential for the *in vitro* activity against the acute respiratory syndrome coronavirus-2 [3]. FAV was first applied as a medication against COVID-19 in China-Wuhan, at the red zone of the pandemic origin. After that as the pandemic been in Europe, FAV got approval for emergency use in Italy, and currently has been in use in Japan, Russia, and many other countries around the globe including Egypt [4]. The main advantages of using FAV to treat a new indication, a process called “drug repurposing,” are that FAV is available in high doses and the safety measurements have previously been conducted on a high patients number [5,6]. Accordingly, the approved medical agent FAV has the potential to be rapidly used on a large scale and be used as a first line of protection to administer to suspect or contact cases during a pathogen lockdown [5].

Based on the above mentioned facts, there is urgent need to develop a sensitive, reliable, fast, low expensive analytical method to trace and determine FAV individuality and in the presence of co-administered drugs. By reviewing the previously published works regarding the determination of FAV, only few methods have been reported for the determination of FAV including HPLC method [7], and spectrofluorometric method [8]. One electrochemical method has been reported for the single determination of FAV [9].

The MnO_2 nanomaterials have been used in different applications due to their high capacitance and low cost preparation; they are eco-friendly nanomaterials with an extraordinary stability in alkaline solutions [10]. By the incorporation of carbon with a high electrical

* Corresponding authors.
E-mail addresses: nicole.jaffrezic@univ-lyon1.fr (N. Jaffrezic-Renault), abdelhamid.errachid-el-salhi@univ-lyon1.fr (A. Errachid).
[1] Equal first author contribution.

https://doi.org/10.1016/j.jelechem.2021.115422
Received 14 April 2021; Received in revised form 22 May 2021; Accepted 26 May 2021
Available online 28 May 2021

conductivity, the conductivity of MnO_2 nanomaterials were further enhanced, reduce the equivalent resistance and charge-transfer resistance [10–12]. Graphene nanostructured materials have received great attention in the past recent years as these materials offer high conductivity, excellent mechanical characteristics, high chemical/thermal stability, with tremendous surface area [13–16].

So, due to the urgent need to develop a fast, precise and sensitive strategy for the sensitive determination of FAV, we have fabricated the present electrochemical protocol. In this work, hydrothermal one-pot strategy was developed to prepare directly MnO_2-rGO nanocomposite using graphene oxide (GO). To the best of our knowledge, there were no literature reporting the use of MnO_2-rGO nanocomposite for the modification of screen-printing electrodes (SPE) for the electrochemical determination of FAV.

2. Experimental

The whole data and description of the used chemicals, apparatus, and methods are described in the electronic supplementary information (ESI) section S2.

3. Results and Discussion

3.1. Characterization of MnO_2-rGO nanocomposite

The structural morphology of the prepared MnO_2-rGO nanomaterial is displayed in Fig. 1A. TEM photo is used to examine the structural morphology of MnO_2-rGO. TEM displays the structure of graphene with transparent layers and the manganese oxide distribution on its surface, (Fig. 1A). The MnO_2-rGO provided high surface area over the common graphite. The bulky particles of the graphite was exfoliated to layers with higher surface area. While the existence of MnO_2 nanoparticles with particle' diameter in the range of 30–85 nm offer much higher surface area that lead to improving the adsorptive affinity towards the FAV throughout the MnO_2-rGO/SPE surface. Also, the EDX spectrum was utilized to examine the elemental configuration of the prepared material. Fig. 1B shows the EDX of nanocomposite, indicating the presence of Mn, O, and C.

The non-destructive method XRD is a beneficial tool in the description of MnO_2. Inset in Fig. 1B shows different peaks at 2θ 18.10°, 29.0°, 31.14°, 37.50°, 44.54°, 50.68°, 59, 98° and 64.70° [11]. The sharp peaks are confirming the stability of MnO_2 crystalline nanoparticles. The peaks are correlated to 200, 310, 110, 002, 210, 512, 521 and 541 planes of crystalline MnO_2 [17–19], Fig. 1C.

Field Emission Scanning Electron Microscopy (FE-SEM) Fig. 1D displays the hydrothermal synthesized MnO_2 nanoparticles of a spherical shape that covered the rGO surface. Fig. S1 depicts the FTIR of graphene oxide and MnO_2-rGO nanomaterial. By inspection the FTIR spectra of GO, the C═C stretching and C—O—C epoxy stretching peaks appeared at 1642 and 1225 cm^{-1}, while the bands at 1725 and 1054 and 3224–3350 cm^{-1} correspond to C═O stretching, C—O in alkoxy group and OH for the adsorbed H_2O. These FTIR indicate the graphite oxidation [20–23]. While for MnO_2-rGO nanocomposite, epoxy, alkoxy and carbonyl peaks were decreased because of the reduction of GO. Moreover, the clear events at 582 and 468 cm^{-1} are recognized for the MnO_2 nanoparticles that completely cover the reduced graphene sheets [24].

3.2. Electrochemical characterization of the SPE modified with MnO_2-rGO nanocomposite

Next, the electrochemical characteristics of the developed platforms were depicted in 5.0 mM potassium ferricyanide ($K_3Fe(CN)_6$) in 0.1 M KCl. MnO_2-rGO/SPE (1:1) performance was compared to the bare SPE, and GO/SPE, Fig. 2A. The redox peaks for MnO_2-rGO/SPE were 3.33, and 1.62 times higher than those of SPE, and GO/SPE, respectively, which could be attributed to the increase in the surface area of MnO_2-Gr compared to GO. The impedance spectroscopy (EIS) is a potent method for proper specification of the different parameters like mass transport and kinetic as well as the coefficient of charge transfer.

Fig. 2B displays the electrochemical impedance spectroscopy (EIS) plot of bare SPE, GO/SPE, and MnO_2-Gr/SPE platforms, which were detected in 5.0 mM potassium ferricyanide ($K_3Fe(CN)_6$) in 0.1 M KCl. A simple corresponding circuit model was applied to adequate the obtained data.

Rs, C and R_{CT} symbolize solution resistance, a capacitance for the double-layer and electron transfer resistance, respectively. Z_W is a Warburg -type impedance coupled to R_{CT}, which represents the bulk diffusion. A semicircle with a Warburg-type line was shown in the spectra. The reduction in the semicircle diameter was indicated in the Nyquist plot for the electrochemical platforms GO/SPE and MnO_2-rGO/SPE, indicating an enhancement of charge transfer kinetics for those sensors comparing to the unmodified bare SPE.

The capacitance (C) was in parallel with the R_{CT} and W impedance. The resistance of charge transfer R_{CT} was valued to be 5970.0 Ω for the unmodified SPE, while it diminished to 4880.0, and 1600.0 Ω for GO/SPE, and MnO_2-rGO/SPE, respectively, indicating the significantly lower R_{CT} value at the MnO_2-rGO/SPE. The obtained cyclic voltammograms data were in a good agreement with the previous data gained from the electrochemical impedance measurements, showing that MnO_2-rGO offers high area along with good electron conduction.

The value of resistance of charge transfer R_{CT} can be applied to estimate the rate constant of the electron transfer (k^o) through the MnO_2-rGO/SPE. Using the following equation [25]:

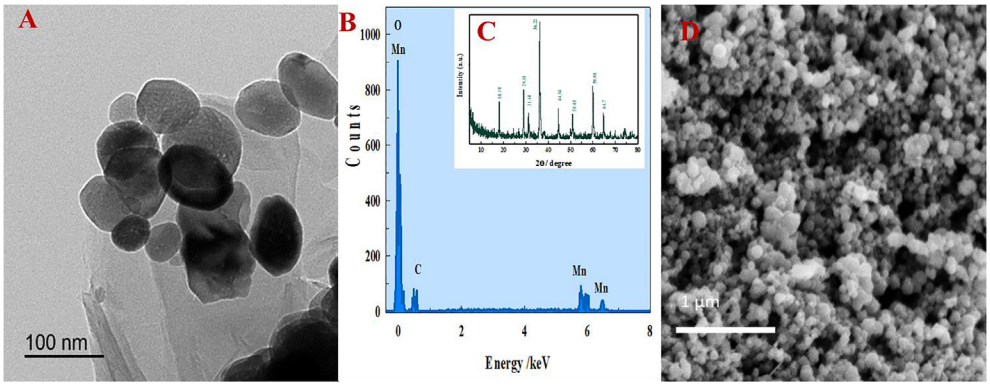

Fig. 1. A) TEM, B) EDX spectra, C) XRD) D) FE-SEM of MnO_2-rGO.

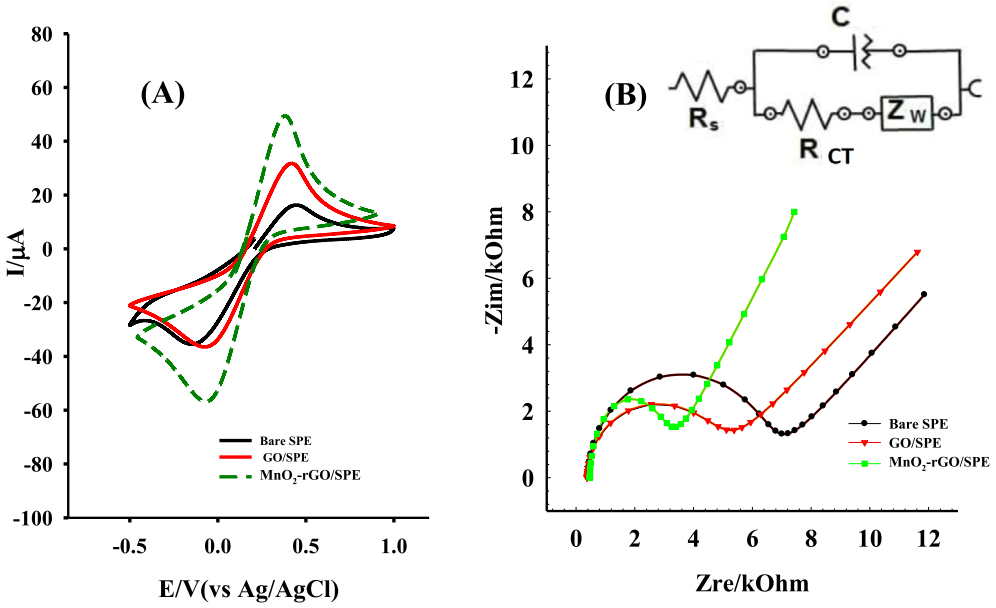

Fig. 2. (A) The recorded CV curves at scan rate (ν) of 0.1 V s^{-1} in 5.0 mM $K_3Fe(CN)_6$ (1:1) in 0.1 M KCl solution at SPE, GO/SPE, and MnO_2-rGO/SPE electrodes, (B) the electrochemical impedance of each electrode.

$k^o = \frac{RT}{F^2 R_{CT} AC}$ where R is defined as the universal gas constant, T is the thermodynamic temperature (298.15 K), F is the Faraday's constant (96485 C mol^{-1}), A is the sensor area and C is the electroactive species concentration in the electrolyte medium. Heterogeneous electron transfer rate constant (k^o) were estimated and the calculated values were: 1.08×10^{-7}, 1.10×10^{-7}, and 1.75×10^{-7} cm s^{-1} for the bare SPE, GO/SPE, and MnO_2-rGO/SPE, respectively.

By comparing the k^o constant values, the highest value of k^o that is related to MnO_2-rGO/SPE indicates the effect of MnO_2-rGO nanomaterial for the enhancement of electron transfer kinetics throughout the electrode surface.

3.3. Electrochemical detection of Favipiravir with the SPE modified with MnO_2-rGO nanocomposite

Fig. 3A displays the characteristic SWV of 5.5×10^{-4} M FAV in pH 7.0B.R. buffer at unmodified SPE, GO/SPE, and MnO_2-rGO/SPE. Upon adding of 1.0 mM FAV, the unmodified SPE showed an anodic peak current of 14.70 μA at 1.27 V, which related to the oxidation of FAV. As can be seen in Fig. 3A, the value of the current of the electrode rises due to the addition of GO, where the anodic peak appears at 1.25 V with a current value of 18.10 μA. After modification of the sensor with MnO_2-rGO, the peak current increased to 25.14 μA at 1.14 V. Consequently, the successful application of MnO_2-rGO for the determination of FAV enhanced the analytical signal, due to a higher electron transfer with high electrical conductivity.

One of the important factors that affect the electrochemical process is the solution pH. Different pH values were tested using 5.5×10^{-4} M FAV, Fig. 3B. Upon varying the pH from 2.0 to 9.0, the FAV oxidation peak was shifted towards lower potentials values, i.e. more negative values, which might be explained as reduction–deprotonation of FAV [26]. The relation between the peak potential (E_p) and pH values of the buffer solution was linear as: E_p (V) = 1.558 V–0.046 V pH^{-1}, (R^2 = 0.9845). The slope value follows Nernst behavior where the included number of electrons and protons are equal during the electrochemical oxidation of FAV. Furthermore, the physiological pH 7.0 was selected as the optimum working one.

Chronoamperometric measurements (CA) at 1.23 V for 20 s were performed for the determination of diffusion coefficient (D) applying Cottrell's law [27], Fig. 4. The calculated D value was found to be 4.67×10^{-5} cm^2 s^{-1} for FAV at MnO_2-rGO/SPE in 0.04 M B.R. buffer (pH 7.0).

3.4. Analytical performance of the SPE modified with MnO_2-rGO nanocomposite

For the determination of FAV, SWV experiments were done using MnO_2-rGO/SPE in solutions of varying FAV concentrations using pH 7.0B.R. buffer. As depicted in Fig. 5A, the calibration curve is drawn as peak current Ip vs. FAV concentration. For the range 1.0×10^{-8}–5.5×10^{-5} M, the regression equation was I(μA) = 0.048C – 1.10; (R^2 = 0.9990). The calculated values for the limit of detection (LOD) and limit of quantification (LOQ) were found to be 9.0×10^{-9} and 2.9×10^{-8} M, respectively.

To check the specificity of MnO_2-rGO/SPE, its electro-analytical response was examined for the determination of FAV in the existence of co-administered COVID-19 drugs including fingolimod, remdesivir, and hydroxychloroquine (HCQ). Fingolimod and remdesivir did not show any electrochemical activity using MnO_2-rGO/SPE. Paracetamol (PAR) also is prescribed for COVID 19 patients for fever control. Fig. 6A shows voltammetric response of FAV in presence of PAR as the peak at 0.43 V is corresponding to PAR, while the other at 1.23 V is due to FAV oxidation. These findings are indicating that the simultaneous determination of the co-administered drugs of FAV is practicable using the MnO_2-Gr/SPE platform. While for testing hydroxychloroquine (HCQ), two separated peaks appeared at 1.01 and 0.81 V at pH 7. Upon adding 5.5×10^{-4} M FAV, FAV well-separated peak appeared at 1.23 V, Fig. 5B. Comparing to the published electrochemical work [9], our sensor offers wide range of linearity and sensitive determination of FAV alone and the presence of different coadministered drugs were demonstrated for the first time.

3.5. Repeatability, reproducibility, and storage stability of the MnO_2-rGO/SPE electrochemical sensor

The MnO_2-rGO/SPE sensor showed high repeatability and reproducibility for FAV analysis. Five determinations of 1.0×10^{-5} M FAV were performed for a single MnO_2-rGO/SPE (intra-day repeatabil-

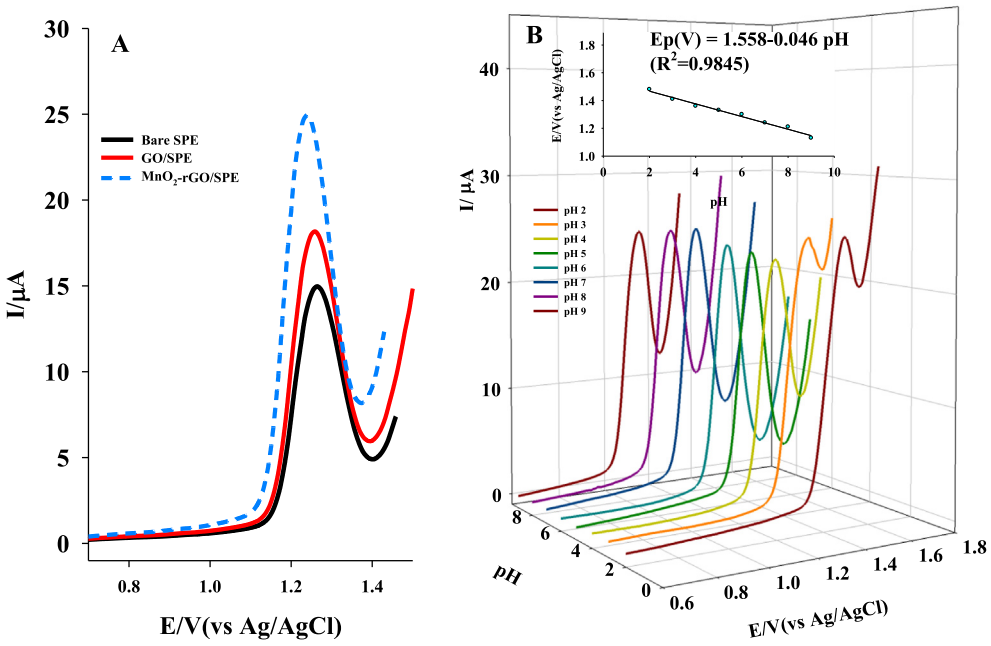

Fig. 3. (A) SWV of 5.5 × 10^{-4} M FAV in B.R. buffer solution pH 7.0 at a SR of 0.1 V s^{-1} at SPE, GO/SPE, and MnO_2-rGO/SPE electrodes, (B) SWV of 5.5 × 10^{-4} M FAV at different pH values using MnO_2-rGO/SPE at ν = 0.1 V s^{-1}, P_W = 0.50 V, P_H = 0.25 V, S_H = 0.02 V. The inset: the plot of I_P *versus* pH.

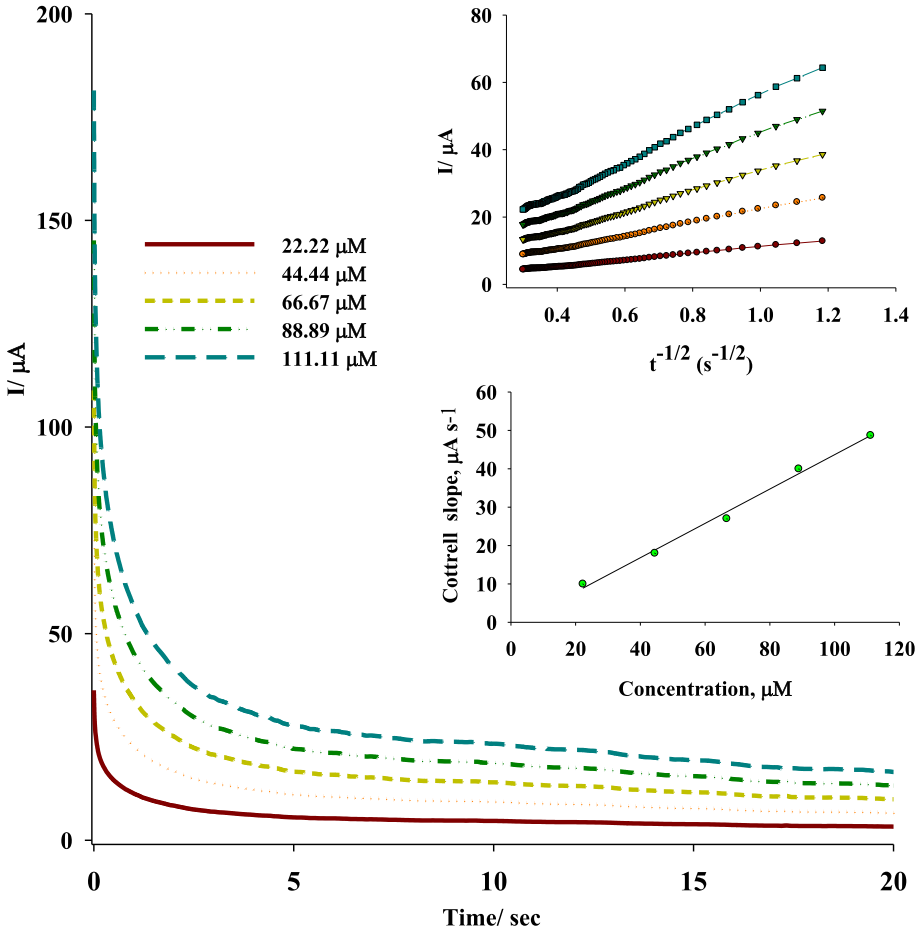

Fig. 4. CA measurements for the oxidation of FAV concentrations using MnO_2-rGO/SPE in B.R buffer pH 7.0, with a P_s = 500 mV. Inset displays the variant of CA currents at t = 20 s vs. [FAV].

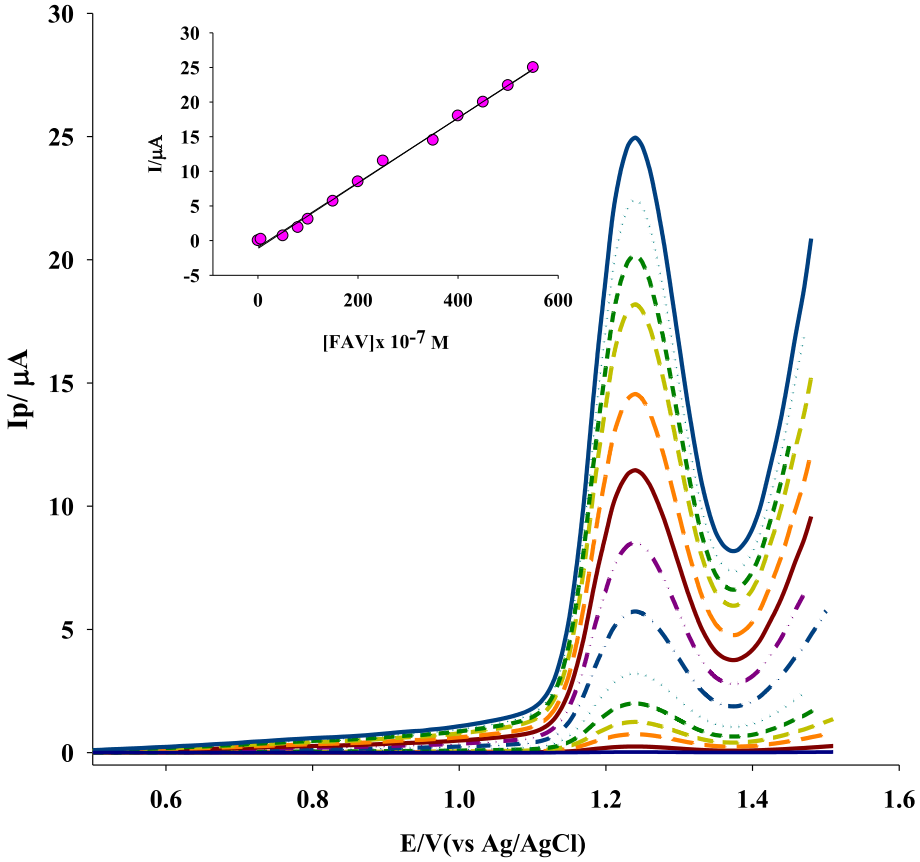

Fig. 5. A) SWVs measurements at MnO_2-rGO/SPE in a pH 7.0B.R. buffer for the concentration range 1.0v10^{-8}–5.5 × 10^{-5} M FAV at ν = 0.1 V s^{-1}, P_W = 0.50 V, P_H = 0.25 V, S_H = 0.02 V. The inset displays the plot of the I_p and FAV concentration in the concentration range 1.0 × 10^{-8} to 5.5 × 10^{-4} M.

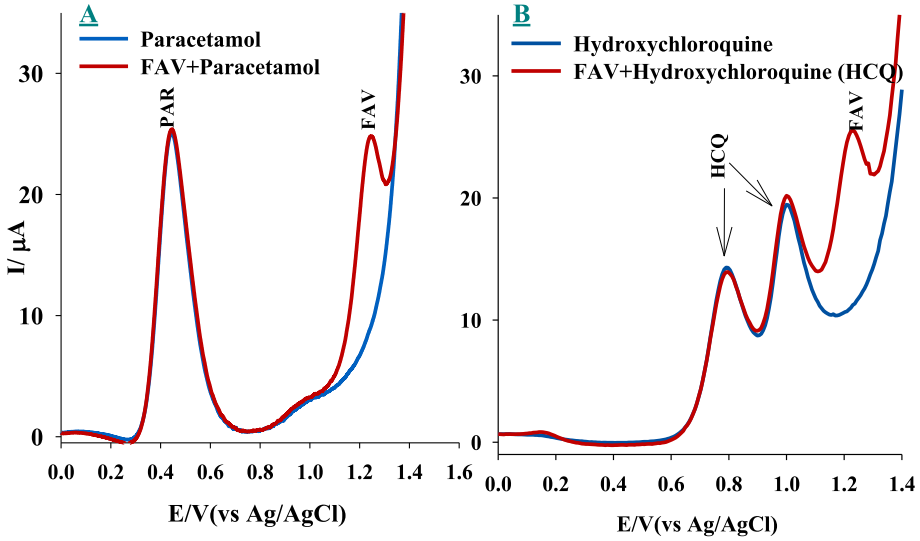

Fig. 6. SWVs of A) HCQ, and FAV B) PAR, and FAV at ν = 0.1 V s^{-1}, P_W = 0.50 V, P_H = 0.25 V, S_H = 0.02 using pH 7.0B.R. buffer.

ity). The relative standard deviation (RSD) for five determinations of FAV was 1.37%. Furthermore, the series of five different MnO_2-rGO/SPE sensors made-up in the same procedure (inter-day reproducibility) have showed the response with an RSD of 1.53% during the electroanalytical determination of 1.0 x10^{-5} M FAV (Fig. S2).

After the preliminary determination of FAV, the MnO_2-rGO/SPE sensor was kept in the buffer (pH = 7.0) at 25 °C. The FAV electrochemical response was checked regularly over 4 weeks (Fig. S2). So, four sensors prepared in the same manner were tested in parallel (n = 3). After four weeks, the final current decreased by 12% of the initial current value that proposes the sensor was rationally stable through the checking period. The high stability of the sensor can be gained because of the hydrophobic property of the graphene materials [28–30], which prevents the formation of a water film on the sensor surface.

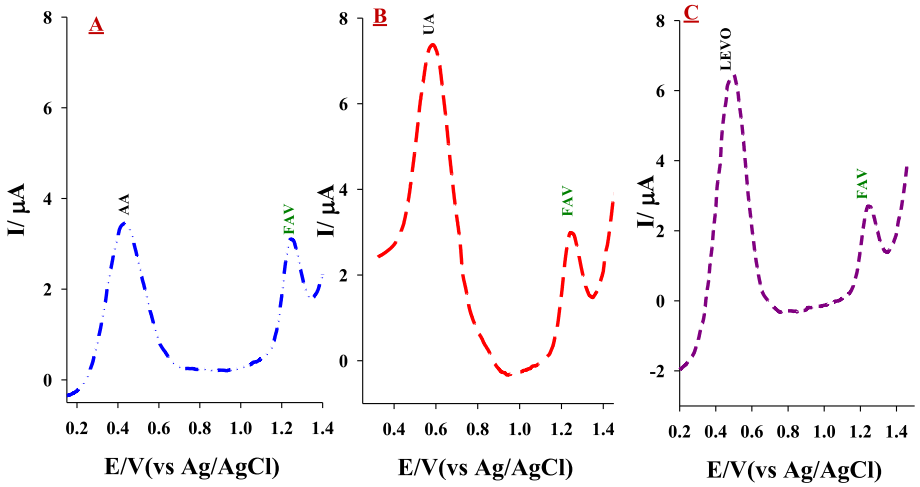

Fig. 7. SWVs using a MnO_2-rGO/SPE in a pH 7.0B-R buffer containing 5.0×10^{-5} M FAV, 5.0×10^{-3} M AA, UA and LEVO, respectively, for each at scan rate: 0.1 V s^{-1}, P_H = 0.25 V, P_W = 0.50 V, S_H = 0.02 V.

Table 1
Determination of FAV in human plasma and synthetic tablets using MnO_2-rGO/SPE.

Sample	Added (µM)	Found (µM)	Recovery%
Plasma	12.00	11.82	98.50
	55.00	54.03	98.23
	120.00	118.92	99.10
	150.00	148.80	99.20
Recovery% ± R.S.D			98.75 ± 0.46
Invisiram® Tablet	12.00	11.88	99.00
	55.00	54.50	99.10
	120.00	118.52	98.77
	150.00	148.99	99.33
Recovery% ± R.S.D			99.05 ± 0.23

3.6. Interference studies

Croscarmellose sodium, sodium lauryl sulphate, titanium dioxide, sodium dihydrogen orthophosphate (H_6NaO_6P), talc, castor oil, mannitol, cellulose, magnesium oxide, and povidone, were examined in order to check any change in the FAV electrochemical signal. Using 1.0×10^{-5} M FAV in a pH 7.0B.R. buffer (0.04 M) solution, each was added, and the magnitude of the anodic peak current was monitored. From the chosen potential interfering substances, none were found to interfere with the electroanalytical sensing of FAV. The tolerance limit was less than ± 5.0% for each interfering substance. Correspondingly, it was found that the use of 40-fold of inorganic ions (e.g. Mg^{2+}, K^+, Zn^{2+}, Na^+, Fe^{3+}, Ca^{2+}, Cl^-, NO_3^- and SO_4^{2-}) did not affect the electrochemical responce, as shown in Fig. S3.

In addition, the important commonly interfering materials in the biological fluids ascorbic acid (vitamin C, AA) and uric acid (UA) have been tested in the presence of 1.0×10^{-5} M FAV. Also, the precursor of dopamine, levodopa (LEVO) has been checked. The high peak potentials separation between the oxidation peaks of these compounds and FAV indicates the promising determination of FAV in biological fluids without interference, Fig. 7.

3.7. Analysis of FAV in real samples

The practicability of MnO_2-rGO/SPE for the determination of FAV in real samples were tested using SWV technique. The standard addition method was used to evaluate the analytical performance of the sensor for FAV determination. The recovery experiment was presented in Table 1, which confirm that, the MnO_2-rGO/SPE is very sensible for the determination of low and high concentrations of FAV in different real samples.

4. Conclusion

In the current study, we have described for the first time, the electrochemical determination of FAV with screen-printed electrode modified with MnO_2-rGO nanocomposite. The developed electrochemical platform showed outstanding electrocatalytic activity towards the sensitive determination of FAV with low values of detection and quantification limits along with wide linearity range. Furthermore, FAV was selectively determined using MnO_2-rGO/SPE platform in the presence of co-administered drugs with high recovery values. Based on the obtained results for the oxidation of FAV, the quantitative determination of FAV in pharmaceutical preparation and human fluids samples was achieved by a simple, rapid, selective and sensitive SWV technique. Furthermore, along with the excellent characteristics of high accuracy, sensitivity, and reproducibility, the developed sensor offers appropriate simple platform for the sensitive determination of FAV in the clinical work.

CRediT authorship contribution statement

Mona A. Mohamed: Investigation. **Ghada M. G. Eldin:** Investigation. **Sani M. Ismail:** Investigation. **Nadia Zine:** Writing - original draft preparation. **Abdelhamid Elaissari:** Conceptualization. **Nicole Jaffrezic-Renault:** Writing - review and editing. **Abdelhamid Errachid:** Funding acquisition, Writing - review and editing.

Declaration of Competing Interest

The authors declare that they have no known competing financial interests or personal relationships that could have appeared to influence the work reported in this paper.

Acknowledgments

The authors acknowledge the partial funding from KardiaTool, H2020, under the grant number 768686 and POC Allergies through the ERA PerMed program. Mona A. Mohamed thanks the French Embassy in Egypt for supporting this work. Campus France is acknowledged for financial support through PHC Imhotep # 46354WG.

Appendix A. Supplementary data

Supplementary data to this article can be found online at https://doi.org/10.1016/j.jelechem.2021.115422.

References

[1] A. Shannon, B. Selisko, N.-T.-T. Le, J. Huchting, F. Touret, G. Piorkowski, V. Fattorini, F. Ferron, E. Decroly, C. Meier, B. Coutard, O. Peersen, B. Canard, Rapid incorporation of Favipiravir by the fast and permissive viral RNA polymerase complex results in SARS-CoV-2 lethal mutagenesis, Nat. Commun. 11 (1) (2020) 4682.

[2] S. Flaxman, S. Mishra, A. Gandy, H.J.T. Unwin, T.A. Mellan, H. Coupland, C. Whittaker, H. Zhu, T. Berah, J.W. Eaton, M. Monod, P.N. Perez-Guzman, N. Schmit, L. Cilloni, K.E.C. Ainslie, M. Baguelin, A. Boonyasiri, O. Boyd, L. Cattarino, L.V. Cooper, Z. Cucunubá, G. Cuomo-Dannenburg, A. Dighe, B. Djaafara, I. Dorigatti, S.L. van Elsland, R.G. FitzJohn, K.A.M. Gaythorpe, L. Geidelberg, N.C. Grassly, W.D. Green, T. Hallett, A. Hamlet, W. Hinsley, B. Jeffrey, E. Knock, D.J. Laydon, G. Nedjati-Gilani, P. Nouvellet, K.V. Parag, I. Siveroni, H.A. Thompson, R. Verity, E. Volz, C.E. Walters, H. Wang, Y. Wang, O.J. Watson, P. Winskill, X. Xi, P. G.T. Walker, A.C. Ghani, C.A. Donnelly, S. Riley, M.A.C. Vollmer, N.M. Ferguson, L. C. Okell, S. Bhatt, C.-R.T. Imperial College, Estimating the effects of non-pharmaceutical interventions on COVID-19 in Europe, Nature 584(7820) (2020) 257-261.

[3] S. Joshi, J. Parkar, A. Ansari, A. Vora, D. Talwar, M. Tiwaskar, S. Patil, H. Barkate, Role of favipiravir in the treatment of COVID-19, Int. J. Infect. Dis. 102 (2021) 501–508.

[4] U. Agrawal, R. Raju, Z.F. Udwadia, Favipiravir: A new and emerging antiviral option in COVID-19, Med. J. Armed Forces India 76 (4) (2020) 370–376.

[5] V. Madelain, F. Mentré, S. Baize, X. Anglaret, C. Laouénan, L. Oestereich, T.H.T. Nguyen, D. Malvy, G. Piorkowski, F. Graw, Modeling favipiravir antiviral efficacy against emerging viruses: from animal studies to clinical trials, CPT: Pharmacometrics & Systems Pharmacology (2020).

[6] S. Pushpakom, F. Iorio, P.A. Eyers, K.J. Escott, S. Hopper, A. Wells, A. Doig, T. Guilliams, J. Latimer, C. McNamee, Drug repurposing: progress, challenges and recommendations, Nat. Rev. Drug Discovery 18 (1) (2019) 41–58.

[7] İ. Bulduk, HPLC-UV method for quantification of favipiravir in pharmaceutical formulations, Acta Chromatographica (2020).

[8] S.M. Megahed, A.A. Habib, S.F. Hammad, A.H. Kamal, Experimental design approach for development of spectrofluorimetric method for determination of favipiravir; a potential therapeutic agent against COVID-19 virus: Application to spiked human plasma, Spectrochim. Acta Part A Mol. Biomol. Spectrosc. 249 (2021) 119241, https://doi.org/10.1016/j.saa.2020.119241.

[9] S. Allahverdiyeva, O. Yunusoğlu, Y. Yardım, Z. Şentürk, First electrochemical evaluation of favipiravir used as an antiviral option in the treatment of COVID-19: A study of its enhanced voltammetric determination in cationic surfactant media using a boron-doped diamond electrode, Anal. Chim. Acta 1159 (2021) 338418.

[10] Y. Sun, W. Zhang, D. Li, L.i. Gao, C. Hou, Y. Zhang, Y. Liu, Facile synthesis of MnO_2/rGO/Ni composite foam with excellent pseudocapacitive behavior for supercapacitors, J. Alloy. Compd. 649 (2015) 579–584.

[11] F.M. El-badawy, M.A. Mohamed, H.S. El-Desoky, Fabrication of an electrochemical sensor based on manganese oxide nanoparticles supported on reduced graphene oxide for determination of subnanomolar level of anti-hepatitis C daclatasvir in the formulation and biological models, Microchem. J. 157 (2020) 104914.

[12] J. Yang, L. Lian, H. Ruan, F. Xie, M. Wei, Nanostructured porous MnO_2 on Ni foam substrate with a high mass loading via a CV electrodeposition route for supercapacitor application, Electrochim. Acta 136 (2014) 189–194.

[13] D.K. Padhi, A. Baral, K. Parida, S.K. Singh, M.K. Ghosh, Visible light active single-crystal nanorod/needle-like α-MnO_2@ RGO nanocomposites for efficient photoreduction of Cr (VI), J. Phys. Chem. C 121 (11) (2017) 6039–6049.

[14] H. Liu, Z. Hu, Y. Su, H. Ruan, R. Hu, L. Zhang, MnO2 nanorods/3D-rGO composite as high performance anode materials for Li-ion batteries, Appl. Surf. Sci. 392 (2017) 777–784.

[15] M.A. Mohamed, S.A. Atty, H.A. Merey, T.A. Fattah, C.W. Foster, C.E. Banks, Titanium nanoparticles (TiO_2)/graphene oxide nanosheets (GO): an electrochemical sensing platform for the sensitive and simultaneous determination of benzocaine in the presence of antipyrine, Analyst 142 (19) (2017) 3674–3679.

[16] M.A. Mohamed, S.A. Atty, N.N. Salama, C.E. Banks, Highly selective sensing platform utilizing graphene oxide and multiwalled carbon nanotubes for the sensitive determination of tramadol in the presence of co-formulated drugs, Electroanalysis 29 (4) (2017) 1038–1048.

[17] F. Xue, S. Wu, M. Wang, J. Wang, A three-dimensional graphene/CNT/MnO2 hybrid as supercapacitor electrode, Integr. Ferroelectr. 190 (1) (2018) 156–163.

[18] L. Feng, Z. Xuan, H. Zhao, Y. Bai, J. Guo, C.-W. Su, X. Chen, MnO 2 prepared by hydrothermal method and electrochemical performance as anode for lithium-ion battery, Nanoscale Res. Lett. 9 (1) (2014) 290.

[19] R.S. Kalubarme, M.-S. Cho, K.-S. Yun, T.-S. Kim, C.-J. Park, Catalytic characteristics of MnO_2 nanostructures for the O2 reduction process, Nanotechnology 22 (39) (2011) 395402, https://doi.org/10.1088/0957-4484/22/39/395402.

[20] N.A. Kumar, S. Gambarelli, F. Duclairoir, G. Bidan, L. Dubois, Synthesis of high quality reduced graphene oxide nanosheets free of paramagnetic metallic impurities, J. Mater. Chem. A 1 (8) (2013) 2789–2794.

[21] D. Kumar, C.M. Raghavan, C.h. Sridhar, J.-H. Shin, S.H. Ryu, K. Jang, D.-S. Shin, Microwave assisted synthesis, characterization of reduced graphene oxide, and its antibacterial activity, Bull. Korean Chem. Soc. 36 (8) (2015) 2034–2038.

[22] W. Sun, S. Shi, T. Yao, Graphene oxide-Ru complex for label-free assay of DNA sequence and potassium ions via fluorescence resonance energy transfer, Anal. Methods 3 (11) (2011) 2472–2474.

[23] P. Divya, S. Ramaprabhu, Platinum-graphene hybrid nanostructure as anode and cathode electrocatalysts in proton exchange membrane fuel cells, J. Mater. Chem. A 2 (14) (2014) 4912–4918.

[24] S. Saha, A. Pal, Microporous assembly of MnO_2 nanosheets for malachite green degradation, Sep. Purif. Technol. 134 (2014) 26–36.

[25] E.P. Randviir, C.E. Banks, Electrochemical impedance spectroscopy: an overview of bioanalytical applications, Anal. Methods 5 (5) (2013) 1098–1115.

[26] G. Ziyatdinova, E. Ziganshina, H. Budnikov, Electrochemical reduction and quantification of menadione in sodium dodecyl sulfate micellar media, J. Solid State Electrochem. 17 (10) (2013) 2679–2685.

[27] A.J. Bard, L.R. Faulkner, J. Leddy, C.G. Zoski, Electrochemical Methods: Fundamentals and Applications, wiley New York, 1980.

[28] J. Ping, Y. Wang, Y. Ying, J. Wu, Application of electrochemically reduced graphene oxide on screen-printed ion-selective electrode, Anal. Chem. 84 (7) (2012) 3473–3479.

[29] M.A. Mohamed, D.M. El-Gendy, N. Ahmed, C.E. Banks, N.K. Allam, 3D spongy graphene-modified screen-printed sensors for the voltammetric determination of the narcotic drug codeine, Biosens. Bioelectron. 101 (2018) 90–95.

[30] M.A. Mohamed, A.M. Yehia, C.E. Banks, N.K. Allam, Novel MWCNTs/graphene oxide/pyrogallol composite with enhanced sensitivity for biosensing applications, Biosens. Bioelectron. 89 (2017) 1034–1041.